International Journal of Nanomedicine

Dovepress
open access to scientific and medical research

Open Access Full Text Article

ORIGINAL RESEARCH

# Solubilisation and Enhanced Oral Absorption of Curcumin Using a Natural Non-Nutritive Sweetener Mogroside V

Junying Zhang[1,*], Yiwen Zhang[1,*], Hufang Wang[1], Wenlin Chen[1], Aiyu Lu[1], Hailiang Li[1], Lifeng Kang[2], Chunyong Wu[3]

[1]Department of TCMs Pharmaceuticals, China Pharmaceutical University, Nanjing, People's Republic of China; [2]School of Pharmacy, Faculty of Medicine and Health, University of Sydney, Pharmacy and Bank Building A15, Camperdown, Australia; [3]Department of Pharmaceutical Analysis, China Pharmaceutical University, Nanjing, People's Republic of China

*These authors contributed equally to this work

Correspondence: Lifeng Kang, Email lifeng.kang@sydney.edu.au; Chunyong Wu, Email cywu@cpu.edu.cn



**Background:** Curcumin (CUR) is a functional ingredient from the spice turmeric. It has attracted considerable attention recently, owing to its diverse biological activities. However, curcumin has low water solubility, which limited its applications. Some sugar molecules were found to be able to solubilise poorly water-soluble compounds by forming micelles in aqueous solutions.

**Purpose:** To improve the water solubility and oral absorption of CUR, using a non-nutritive natural sweetener, namely, Mogroside V (Mog-V).

**Methods:** A solid dispersion of CUR in Mog-V was prepared using a solvent evaporation method. The solid dispersion was characterised by using X-ray diffraction and differential scanning calorimetry. The solid dispersion can dissolve in water to form micelles with a diameter of ~160 nm, which were characterised by using dynamic light scattering. To find out the mechanism of solubilisation, the aggregation behaviour of Mog-V molecules in aqueous solution was investigated using nuclear magnetic resonance spectroscopy. Finally, oral absorption of CUR in the solid dispersion was evaluated using a rodent model.

**Results:** A solid dispersion was formed in a ratio of 1 CUR to 10 Mog-V by weight. Upon dissolution into water, CUR laden micelles formed via self-assembly of Mog-V molecules, which increased the solubility of CUR by nearly 6000 times compared with pure CUR crystals. In rats, the solid dispersion increased the oral absorption of CUR by 29 folds, compared with CUR crystals. In terms of solubilisation mechanism, it was found that Mog-V self-assembled into micelles with a core-shell structure and CUR molecules were incorporated into the hydrophobic core of the Mog-V micelles.

**Conclusion:** Mog-V can form a solid dispersion with CUR. Upon dissolution in water, the Mog-V in the solid dispersion can self-assemble into micelles, which solubilise CUR and increase its oral absorption.

**Keywords:** Mogroside V, curcumin, micelle, solubilisation, bioavailability, solid dispersion

## Introduction

Curcumin (CUR) is a hydrophobic polyphenol derived from the rhizome of the widely utilised spice turmeric (*Curcuma longa*).[1,2] It has diverse biological activities, such as anti-inflammation,[3] antioxidation,[4] antiproliferation[5] and anti-tumor.[6] The proven clinical safety and efficacy of CUR make it a popular functional food ingredient.[7] However, the oral absorption of CUR is limited by its poor solubility (0.25 μg/mL in water). To address these issues, a number of formulation strategies have been developed, such as solid dispersions,[8] cyclodextrins,[9] microemulsions,[1] nanoparticles,[10] liposomes,[11] and micelles[12] (Table 1).

One way to solubilise CUR is to formulate CUR into nanoscale formulations, such as nano-spheres and nano-capsules.[13] Among nano-formulations, micelles are self-aggregated colloids formed by amphiphilic molecules.[14] Below a certain concentration, namely, critical micellar concentration (CMC), the amphiphilic molecules exist as single

Received: 28 October 2022
Accepted: 2 February 2023
Published: 23 February 2023

**Graphical Abstract**

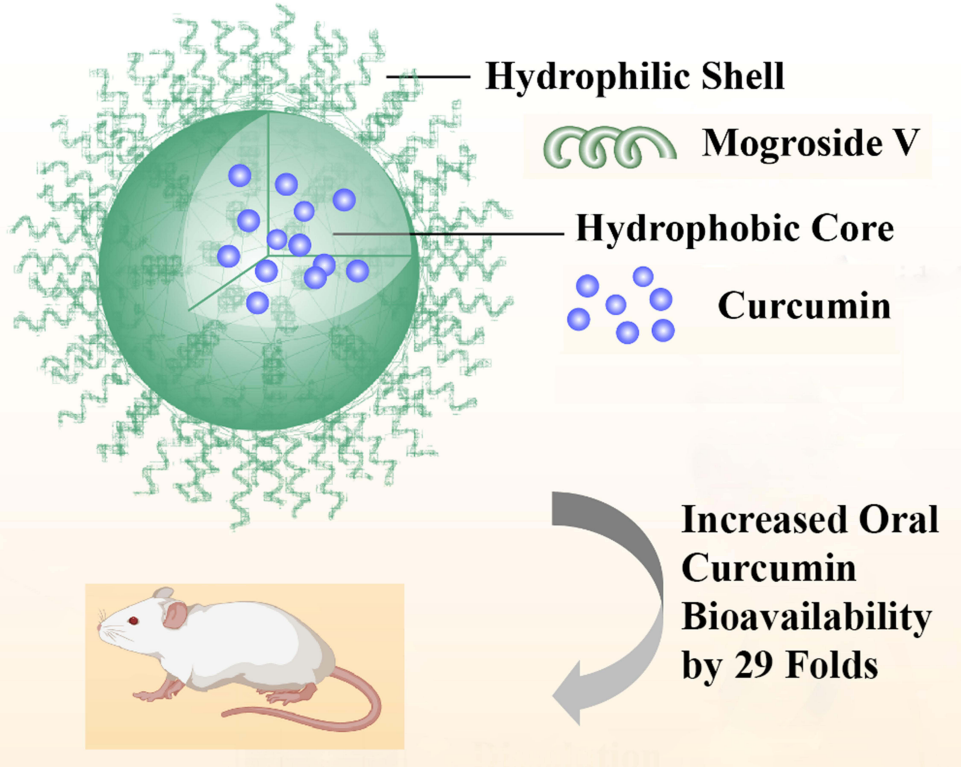


molecules. When their concentration exceeds the CMC, the molecules self-assemble into micelles, which consist of a lipophilic core and a hydrophilic shell. Drug molecules can be encapsulated inside the lipophilic core to achieve increased solubility and absorption into human. As a nanoscale drug delivery system, the advantage of micelle is its

**Table 1** Solubilisation of CUR Using Different Formulations

| Preparation | Formulation | Fold Change Solubility | Fold Change Bioavailability | Ref. |
|---|---|---|---|---|
| Solid dispersions | CUR: Mog-V=1:10<br>CUR: HPMC=1:1<br>CUR:TPGS: mannitol= 1:10:15 | 6712<br>-<br>- | 29<br>17<br>65 | -<br>[8]<br>[36] |
| Cyclodextrins | β-CD | 2.3 | - | [9] |
| Microemulsions | Kolliphor RH40 | - | 4.0 | [37] |
| Nanoparticles | TPGS, Brij78 | - | 12.3 | [38] |
| Liposomes | TMC<br>Carbopol | -<br>- | 1.6<br>2.2 | [39]<br>[40] |
| Micelles | Pluronic | - | - | [12] |

**Abbreviations**: HPMC, Hydroxypropyl Methylcellulose; β-CD, β-Cyclodextrin; TPGS, D-Alpha-Tocopheryl Poly (Ethylene Glycol) Succinate 1000; Brij78, Alkyl-PEO; TMC, N-Trimethyl Chitosan Chloride.

relatively small size of a few hundred nanometres and simple preparation methods that are scalable to industrial manufacturing.[14] Non-ionic surfactants, such as Pluronic, can form micelles in aqueous solutions.[12] The micelles and/or vesicles can be prepared by thin film hydration or heating methods. However, surfactants may not be preferable for oral applications, though they can be used in topical products to enhance skin permeability. Apart from non-ionic surfactants, certain sugar molecules can also form micelles to solubilise CUR and other poorly water-soluble compounds. Many compounds with low water solubility showed pronounced improvement in their solubility after being co-formulated with glycosides, as shown in Table 2.

To prepare solid dispersions, commonly used methods include solvent evaporation, hot melting, and mechanical milling.[15] For hot melting method, the elevated temperature may cause degradation of the active pharmaceutical ingredient and excipients. For milling methods, though no solvent or high temperature is involved, specialised equipment is needed, which may not be readily available. Solvent evaporation method, on the other hand, is easy to perform, especially when ethanol is used to minimise potential hazards from organic solvent residues.

Previously, we studied the solubilisation effects of glycosylated hesperidin,[16] glycosylated rutin,[17] and glycosylated stevia.[18] The glycosylated compounds were prepared by trans-glycosylating the parent sugar molecules using an enzyme, namely, cyclomaltodextrin glucanotransferase, via a complex process.

Alternatively, we can also use glycosidic ingredients extracted from plants.[19,20] Among them, Mogroside V (Mog-V), the main triterpene saponin compound extracted from *Siraitia grosvenorii*, has been shown to be effective to solubilise silybins, a natural flavonoid from the plant milk thistle (Figure 1A).[19] As a non-nutritive sweetener, Mog-V is found in monk fruit and has the status of Generally Recognised as Safe (GRAS) according to US-FDA (United States - Food and Drug Administration).[21]

Non-nutritive sweeteners become increasingly popular as food additives, owing to their potential health benefit of reduced calorie intake. But synthetic sweeteners can lead to intestinal microbiome imbalance and glucose intolerance, causing metabolic system disorders.[22,23] Natural sweeteners, on the other hand, such as stevioside, were better tolerated in human.[23]

Recently, we found that Mog-V can increase the water solubility of silybin, from 1 μg/mL to 2000 μg/mL, a 2000-fold increment.[19] This was achieved by mixing a small amount of silybin with a large portion of Mog-V to form a solid dispersion, which was then dissolved in water. It was postulated that mog-V could form micelles, which encapsulated silybin in the aqueous solution.

The findings have motivated us to investigate Mog-V further to find its solubilisation capability for other compounds with poor water solubility. In addition, we are also interested to study its mechanism of solubilisation via micelle formation in aqueous solutions. CUR was selected as a model compound owing to its significance in food industry and its well-known poor water solubility (Figure 1B). We hypothesise that Mog-V can self-assemble into micelles with core-shell structure to solubilise CUR in the hydrophobic inner core of the micelle (Figure 1C), with a similar mechanism to those glycosylated sugar compounds for solubilisation.

To test our hypothesis, we first prepared the solid dispersion powders (SDPs) of Mog-V and CUR. The SDPs were characterised by using powder X-ray diffractometry (PXRD) and differential scanning calorimetry (DSC), to verify if the CUR has been dispersed and distributed inside Mog-V at molecular level. Afterwards, the SDPs were dissolved in deionised water and the aggregation behaviour of Mog-V in the aqueous solution was assessed by studying the concentration-dependent chemical shift changes. Then $^{1}$H nuclear magnetic resonance (NMR) and two-dimensional (2D) $^{1}$H-$^{1}$H nuclear Overhauser effect spectroscopy (NOESY) were employed to evaluate the spatial localisation of CUR and discussed the solubilisation mechanism of Mog-V for CUR. Lastly, we tested the oral absorption of the SDPs in rats and measured the concentration of CUR in plasma.

# Methods and Materials

## Materials

CUR was purchased from Sigma-Aldrich (St. Louis, MO, USA). Glibenclamide, used as the internal standard (IS) in plasma assay, was bought from Tansoole (TCI, China). Mogroside V (Mog-V, MW = 1287.43) was provided by Chengdu Biopurify Phytochemicals Ltd. (Chengdu, China). All other chemicals and solvents were of analytical grade and used without further purification.

**Table 2** Studies Using Glycosides to Solubilise Poorly Water-Soluble Drugs

| Glycoside | Molecular Weight | CMC (mg/mL) | Active Ingredients to Glycoside Ratio (w/w) | Micelle Size (nm) | Solubility (mg/mL) | Enhancement Ratio of Solubility[a] | Enhancement Ratio of AUC[a] | Reference |
|---|---|---|---|---|---|---|---|---|
| Hesperidin-G | 772.7 | 5.0 | Naringenin: Hesperidin-G =1:20 | - | 3.5± 0.2 | 77 | - | [41] |
| | | | Flurbiprofen: Hesperidin-G =1:10 | - | 0.5 | 10 | 2.8 | [42] |
| | | | Probucol: Hesperidin-G =1:10 | - | 0.005 | 1000 | 5.3 | [43] |
| | | | Glibenclamide: Hesperidin-G =1: 5 | - | - | - | 6 | [44] |
| | | | Naringenin: Hesperidin-G =1:10 | - | 1.4 | 30 | - | [16] |
| Rutin-G | 759 | 5.0 | Tranilast: Rutin-G=1:10 | 2.9 | 0.04 | 32.2 | 36.4 | [45] |
| | | | Ipriflavone: Rutin-G=1:10 | - | 0.003 | 3 | 4.3 | [46] |
| | | | Folic acid: Rutin-G= 1:2 | <100 | 1 | 100 | - | [47] |
| | | | Flurbiprofen: Rutin-G =1:10 | - | - | - | 2.2 | [17] |
| Stevia-G | 965.0 | 12 | Propolis: Stevia-G =1:10 | 350 | - | - | 6.4 | [48] |
| | | | Curcumin: Stevia-G=1:10 | - | 0.5 | 1600 | - | [29] |
| | | | Curcumin: Stevia-G: PVP K-30=1:10:0.5 | - | 4.1 | 13,000 | 6.7 | [29] |
| | | | Indomethacin: Stevia-G=1:10 | - | 0.04 | 5 | - | [49] |
| | | | Flurbiprofen: Stevia-G=1:10 | - | 0.06 | 1.6 | 2.2 | [43] |
| | | | Probucol: Stevia-G=1:10 | - | 0.007 | 1340 | 9.8 | [43] |
| | | | Mefenamic acid: Stevia-G: LTAC=1:10:1 | - | - | - | - | [50] |
| | | | Naringenin: Stevia-G=1:10 | 3 | 1.8 | 36 | - | [18] |
| | | | Quercetin: Stevia-G: PVP =1:10:5 | - | 0.1 | 5 | - | [51] |
| Stevioside | 804.9 | 4.9 | - | 4.7 | 1.0 | 45 | - | [52] |
| Rebaudioside A | 967.0 | - | Naringenin: Rebaudioside A=1:24 | 5.2 | 24.6 | 2198 | 2.1 | [53] |
| Mogroside V | 1287.4 | 5.5 | Silybin: Mog-V =1:20 | 206 | 2.2 | 1931 | 24.5 | [19] |
| | | | Curcumin: Mog-V=1:10 | 154 | 1.4 | 5712 | 29 | - |
| ssβ-glucan | - | - | Quercetin: ssβ-glucan=1:10 | - | - | - | - | [54] |
| Naringin-G | 742.5 | - | Pranlukast hemihydrate: Naringin-G =1:5 | 2.7 | - | - | 2.2 | [55] |
| Rubusoside | 642.7 | - | Curcumin: Rubusoside=1:20 | 8 | 2.3 | 2318 | - | [20] |

**Note**: [a]After Solubilisation /Untreated Drug.

**Abbreviations**: PVP, Polyvinylpyrrolidone; Hesperidin-G, α-Glucosyl Hesperidin; Rutin-G, α-Glycosyl Rutin; Stevia-G, α-Glucosyl Stevia; Naringin-G, α-Glycosylated Naringin; LTAC, Lauryl Trimethyl Ammonium Chloride.

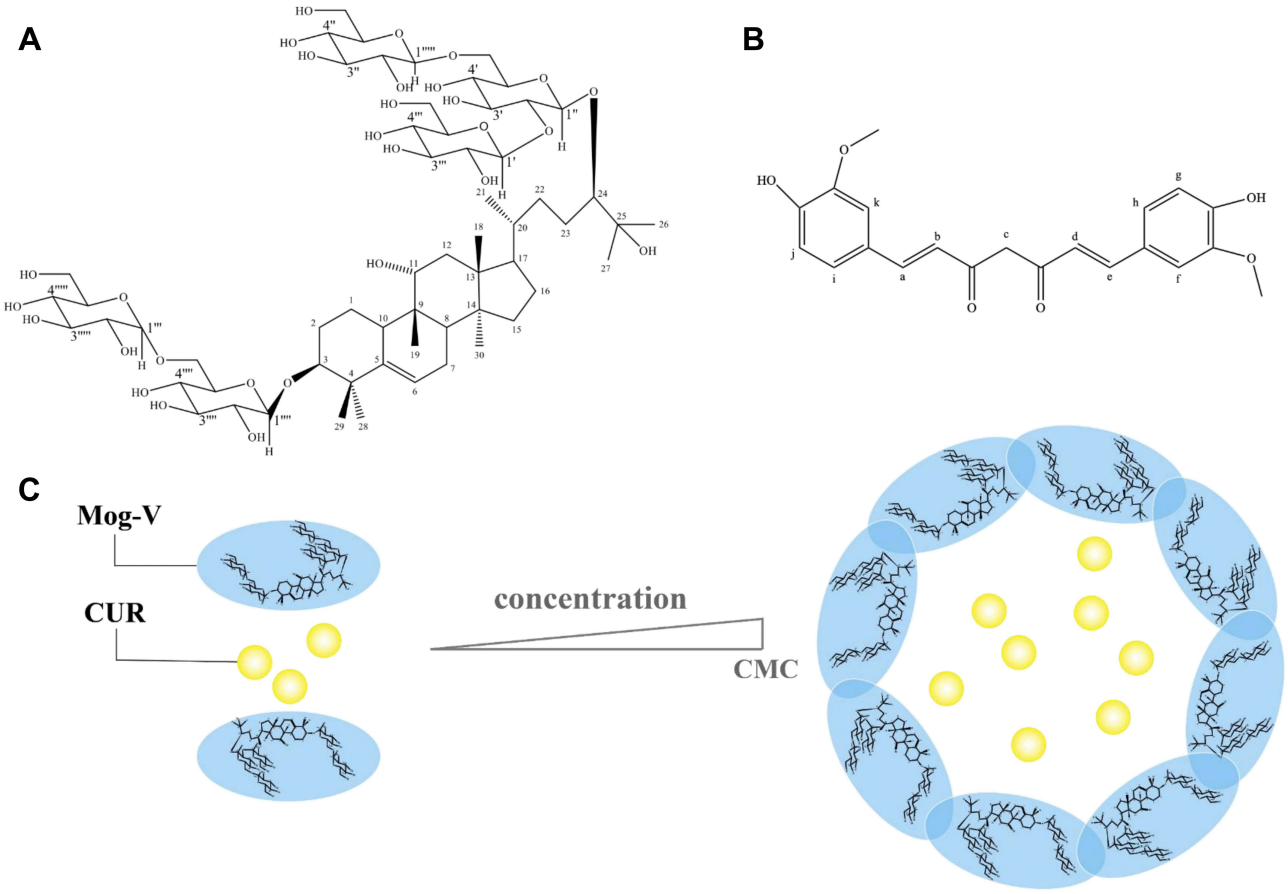


**Figure 1** Chemical structures of (**A**) Mogroside V (Mog-V) and (**B**) Curcumin (CUR) with protons of representative chemical shifts numbered. Schematic representation of the solubilisation mechanism: self-assembly of Mog-V micelles in aqueous solution to encapsulate CUR (**C**).

## Preparation of Physical Mixtures (PMs) and Solid Dispersion Powders (SDPs)

The PMs were prepared by physically mixing CUR and Mog-V at a weight ratio of 1:10 in a glass vial using a vortex mixer. The CUR/Mog-V SDPs were prepared using a solvent evaporation method. CUR (10 mg) and Mog-V (100 mg) were dissolved in the ethanol/water solution (4:1 v/v) with sonication (KQ-250DE Sonorex, Jiangsu, China), followed by rotary evaporation (EYELA N-1100, Shanghai, China) in a water bath at 50 °C for 1 h to remove the solvent. All the powders were stored in a desiccator before their physicochemical properties were tested.

## Powder X-Ray Diffraction (PXRD)

PXRD analysis of all samples (CUR, Mog-V, CUR/Mog-V PMs, and CUR/Mog-V SDPs) was performed at ambient temperature using the D8 X-ray diffractometer system (Bruker AXS, Madison, WI, USA) and Cu Kα radiation (generator setting: 40 kV and 40 mA). Diffraction data were collected at the 2θ scanning, ranging from 3° to 40° with the scanning speed of 4°/min.

## Differential Scanning Calorimetry (DSC)

DSC measurements of all samples (CUR, Mog-V, CUR/Mog-V PMs, and CUR/Mog-V SDPs) were performed using a Netzsch Thermal Analysis DSC 204 (NETZSCH, Germany). Accurately weighed sample (5 mg) was placed in standard aluminum pans and heated at a scanning rate of 10 °C/min from 30 to 300 °C under the nitrogen purging gas. Each run was repeated at least twice.

## Particle Size Analysis

The volumetric particle size distribution of the micelle was determined by dynamic light scattering (DLS) method using a NanoBrook Brookhaven 90 Plus Zeta (Brookhaven Instruments Ltd., USA). The Mog-V and CUR/Mog-V SDPs were dispersed in deionised water, respectively, and then sonicated for 2 min before measurements. The mean particle size was the average value of 3 replicates.

## Solubility Measurement

The apparent solubility of crystalline CUR and CUR/Mog-V SDPs was determined in a flask. Excess samples were added in deionised water, and then mixed at 50 strokes/min at 37 °C. After 24 h, the samples were filtered using a membrane syringe filter (pore size = 0.45 μm). The concentration of CUR was determined using a high performance liquid chromatography (HPLC) system (LC-2010C HT, Shimadzu Co., Ltd., Kyoto, Japan). A Phenomenex $C_{18}$ column (4.6 mm × 250 mm, 5 μm) was used, with a mobile phase consisting of 2% glacial acetic acid:methanol (23:77 v/v) at a flow rate of 1 mL/min. The detection wavelength was set at 424 nm. All solubility measurements were performed in triplicates.

## Dissolution Test

The dissolution test was carried out in 100 mL of pH 1.2 and pH 6.8 phosphate buffer solutions (each containing 0.2% Tween 80) under a stirring speed of 50 rpm at 37 °C. The crystalline CUR and CUR/Mog-V SDPs were weighed to keep an equal amount of 2 mg CUR. During the study, 0.5 mL samples were withdrawn at specified time intervals (5, 10, 20, 30, 60, 120, 180, 240 and 300 min), simultaneously replacing the equal volume of the pure medium of 37 °C. The samples were filtered through a 0.45 μm membrane filter and analyzed using the HPLC system as described above. Three replicates for each sample were assayed.

## NMR Measurements

All NMR experiments were performed at 37 °C on a Bruker AVIII-500 NMR spectrometer (Bruker Corporation, Germany). The samples were prepared in $D_2O$. As an external reference, 0.05% 3-(trimethylsilyl) propionic-2,2,3,3-$d_4$ acid sodium salt (TSP) was used to calibrate the NMR chemical shifts. The spectra were analyzed with reference to the internal signal of TSP-d 4 protons at 0 ppm. Resonance assignments for Mog-V were made according to 2D $^{1}$H-$^{1}$H COSY, $^{1}$H-$^{13}$C HMBC, and $^{1}$H-$^{13}$C HMQC NMR spectra and the reference data.[24] The chemical shifts of protons in Mog-V were recorded as a function of the concentrations (1, 2, 3, 4, 5, 8, 10, 15, 20, 30 and 50 mg/mL).

The 2D $^{1}$H-$^{1}$H NOESY spectra for 1.0 and 50 mg/mL Mog-V solutions were measured to check the molecular conformation of Mog-V in the aqueous solution. Under similar conditions, $^{1}$H NMR spectra and 2D $^{1}$H-$^{1}$H NOESY spectra of CUR/Mog-V SDP solutions (concentration equivalent to 50 mg/mL of Mog-V) were also recorded to validate the interaction positions between CUR and Mog-V molecules. The peaks of CUR were assigned based on prior reports.[25]

## Oral Absorption in Rats

Male Sprague-Dawley (SD) rats weighing 200 ± 20 g were obtained from Qinglongshan Ltd. (Nanjing, China). The rats housed under standard conditions were fasted overnight prior to the drug administration, and water could be obtained *ad libitum*. Experimental procedures on animals were undertaken following the National Guidelines and under the approval of the animal care committee of China Pharmaceutical University for project 81473357.

A total of 8 rats were randomly divided into two groups (4 animals in each group) for oral absorption study. Group I received CUR crystals suspended in 0.5% carboxy methyl cellulose by intragastric gavage at a dose of 100 mg/kg, as illustrated in Supplementary Information (SI). Group II was orally administered CUR/Mog-V SDP aqueous solution at the same dose of CUR, which was freshly prepared by dissolving CUR/Mog-V SDPs in deionised water. Blood samples (0.3 mL) were collected immediately from the suborbital vein under light ether anaesthesia and placed in heparinised 1.5 mL polythene tubes at 5, 15, 30, 60, 120 and 240 min post dosing. Each blood sample was immediately centrifuged at 14,000 rpm for 10 min and the separated plasma samples were stored at −20 °C until further assay.

## Plasma Sample Assay

The internal standard, namely, 20 μL glibenclamide solution (400 ng/mL), and 130 μL of acetonitrile were added into 50 μL plasma samples after thawing, the mixture was vortexed for 5 min and centrifuged at 14,000 rpm for 10 min. Ten microliters of the supernatant were injected into a LC-MS/MS system for analysis.

The chromatographic separations were performed on a Phenomenex $C_{18}$ column (4.6 mm × 250 mm; 5μm) using an Agilent 1260 Series liquid chromatography (Agilent Technologies, Palo Alto, CA, USA). The column was maintained at room temperature during analysis. The mobile phase consisted of 0.1% formic acid solution and methanol (20: 80, v/v). The flow rate was set at 1 mL/min.

The LC effluent was split and introduced into an Agilent triple quadrupole mass spectrometer (Agilent Technologies, USA). The ESI source was operated in the positive mode. The ion transitions of *m/z* 368.9 → 177.0 (CUR) and *m/z* 494.3 → 369.1 (IS) were chosen for the quantitative analysis while undergoing multiple reaction monitoring (MRM). To separate and determine CUR and IS, the MS analysis detection was optimised when the collision energy was at 20 eV for both analytes. The fragmentors were 110 V for CUR and 135 V for IS, respectively. Other optimal parameters were as follows: dwell time, 300 ms; capillary voltage, 4 kV; cell accelerator voltage, 7 V; gas temperature, 300 °C; nebuliser gas, 15 psi; gas flow, 11 L/min. The data analysis was performed by Agilent Mass Hunter Software.

## Statistical Analysis

The data were analysed using SPSS (version 26.0 for mac). The pharmacokinetic parameters were calculated with the non-compartmental model of DAS software version 3.2.7 (Shanghai, China). The experimental data are presented as mean ± standard deviation (SD).

# Results and Discussion

## Solid State Characterisation

Amorphous solid dispersion (ASD) is a popular strategy to increase the solubility of insoluble drugs.[26] ASD is a single-phase amorphous system, where the active ingredient is molecularly dispersed in an excipient matrix. The amorphous state is responsible for their improved dissolution properties because of its higher Gibbs free energy than the crystalline state, as the drug crystal lattice at amorphous state can be broken freely.[27,28]

Previous work has shown that α-glucosyl stevia and rubusoside could enhance the solubility of CUR.[20,29] In the current study, PXRD was used to confirm the crystalline form of the obtained samples. The PXRD pattern (Figure 2) of crystalline CUR exhibited sharp diffraction peaks, while Mog-V showed a broad amorphous band. The superimposition of the diffraction peaks of CUR and Mog-V was observed in the PXRD pattern of the PMs. For the SDPs, the diffraction peaks disappeared, and a characteristic halo pattern was observed, proving that crystalline CUR was successfully changed into amorphous state, indicating the formation of amorphous solid dispersions.

The PXRD alone may not be sufficient to confirm the amorphous form due to the possibility of formation of small traces of crystallinity and nanocrystals.[30] Therefore, a DSC test was performed to confirm the results. DSC thermograms (Figure 2) revealed the endothermic peak of CUR crystal and Mog-V at a temperature of 178.8 °C and 174.3 °C, respectively. This value is in line with the reported melting temperature of CUR.[31] The DSC curve of the PMs remained as a superimposed DSC pattern of CUR crystal and Mog-V. In contrast, the endothermic peak of SDPs was observed at 152.8 °C, and the melting peak of CUR disappeared, indicating that the crystalline CUR transited to the amorphous state.

## Particle Size Distribution in Aqueous Solutions

In this study, micelles were formed by the self-assembly of Mog-V. The poorly water-soluble CUR molecules were encapsulated in the hydrophobic core and solubilised in the aqueous solution. To find out the Mog-V micelle size distribution, the Mog-V powders and SDPs were added to water, respectively. After the solids were fully dissolved, the micelle size was determined using DLS method. It was found that Mog-V self-aggregated and formed micelles. As shown in Figure 3A, Mog-V molecules without CUR can form micelles with a diameter of ~160 nm. In the presence of CUR, Mog-V also formed micelles with a slightly smaller diameter of ~154 nm.

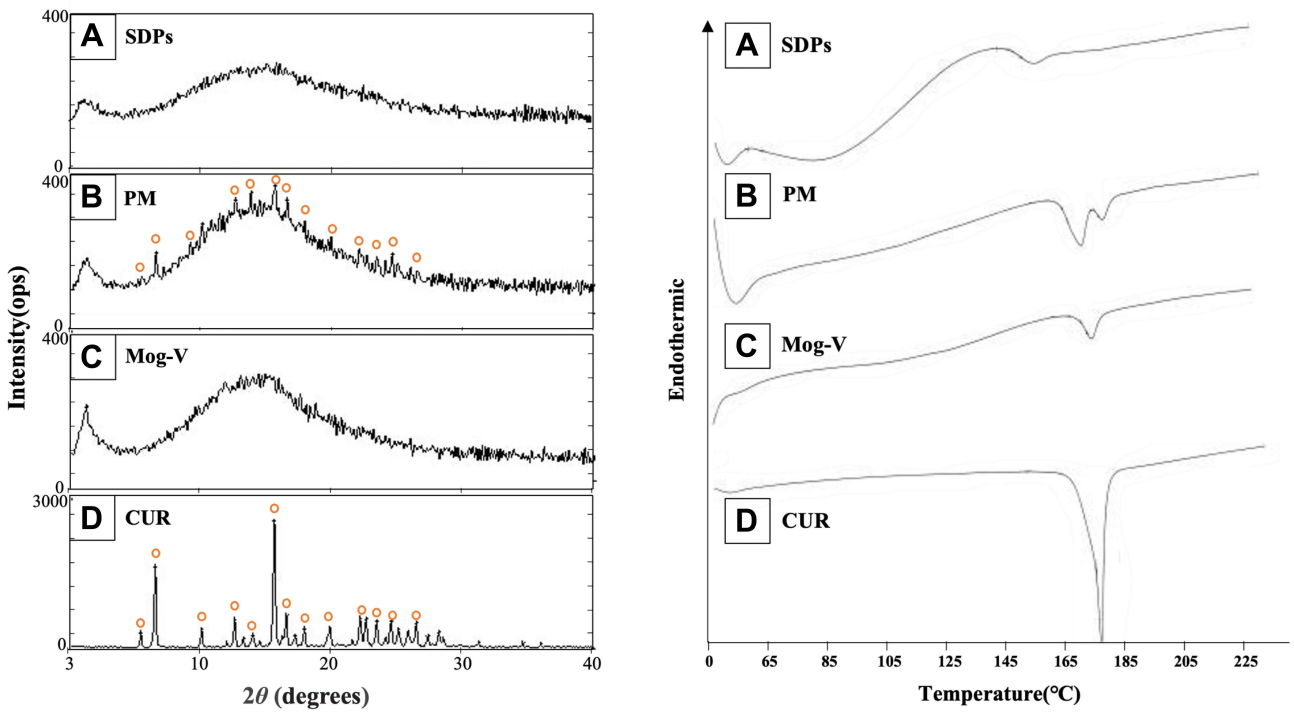


**Figure 2** Power X-ray diffraction diagrams and differential scanning calorimetry thermograms of (**A**) SDPs, (**B**) PMs, (**C**) Mog-V, and (**D**) CUR.

## Solubility & Dissolution Test

The solubility of untreated CUR was determined to be 0.25 μg/mL in deionised water after incubation at 37 °C for 24h, while the solubility of CUR in SDPs dramatically increased to 1428 μg/mL, a 5712-fold increase. The dramatic increase of CUR solubility can be ascribed to the fact that CUR inside SDPs is in amorphous state with higher Gibbs free energy than in crystalline state, and the molecular crystal lattice at amorphous state can be broken freely.

Apart from 24-h solubility, the dissolution rate of CUR was also determined from time 0 to 5 h in both acidic and basic solutions. Figure 3C and D show the dissolution profile of CUR from SDPs in pH 1.2 and pH 6.8 buffer solutions compared to untreated CUR. The dissolution rate of crystalline CUR was slow in pH 1.2 (22% released in 300 min). In contrast, for SDPs, the concentration of dissolved CUR rapidly increased to 54% in 5 min. In the pH 6.8 buffer solution, the trend was similar, i.e., the CUR from SDPs dissolved quickly, while CUR crystal showed a slow dissolution rate.

## Aggregation Behaviour of Mog-V in Aqueous Solutions

To study the aggregation of Mog-V in aqueous solutions, NMR is used. In NMR, the $^{1}H$ chemical shift is often sensitive to subtle changes in the local environment of the molecule and is usually used to study molecular associations.[32] Figure 4A shows the $^{1}H$ NMR spectra of Mog-V at various concentrations. Changes of the chemical shifts of all protons with increased concentrations were observed, partial protons (6) from the tetracyclic triterpenoid skeleton tend to move up-field, while some protons (2) exhibited downfield shifts, confirming the formation of aggregates as the Mog-V concentration increased.

The chemical shift changes were used to calculate the CMC. In this study, the CMC was used as the index parameter of the self-assembly formation. If the concentration is below the CMC, the observed chemical shift ($\delta_{obs}$) is the chemical shift of the pure monomer ($\delta_{mon}$) since the protons are surrounded by solvent molecules. If the concentration is above the CMC, $\delta_{obs}$ is the weighted average of chemical shifts of the monomer and micelle ($\delta_{mic}$) when the exchange of monomers and micelles in the solution is faster than the NMR time scale. In this case, the observed chemical shift is expressed as (Equation 1) using the mass-action law model, where *C* is the total concentration.[33]

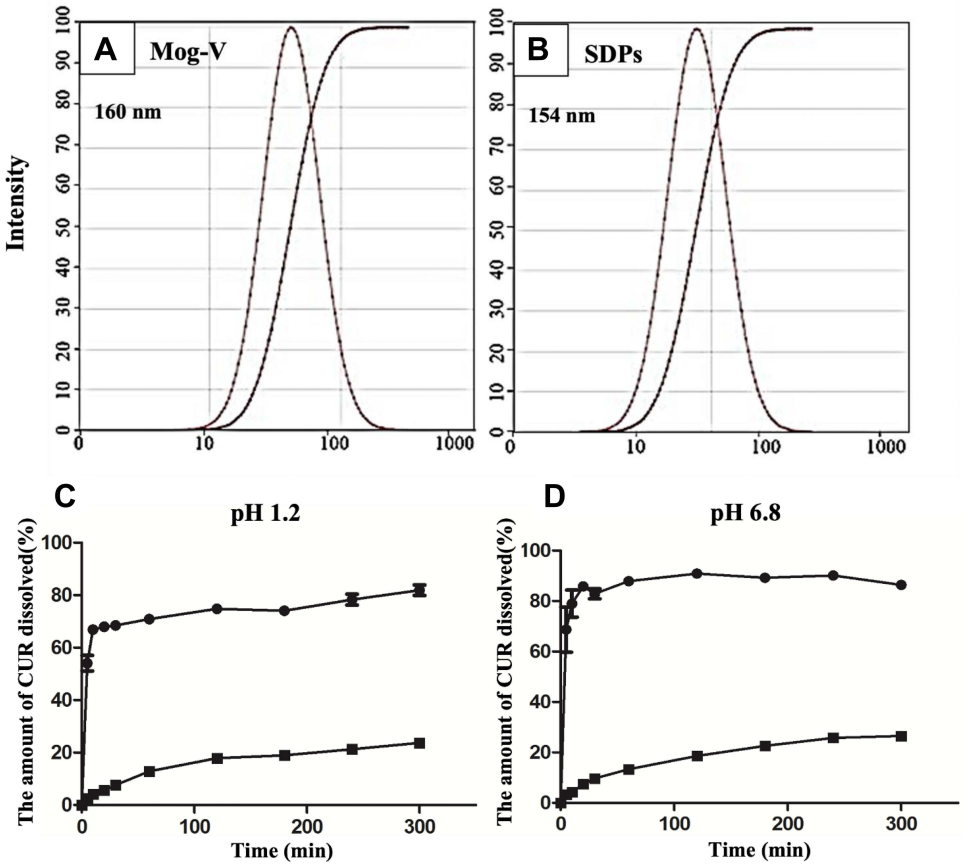


**Figure 3** Particle size distribution of (**A**) Mog-V and (**B**) CUR/Mog-V SDPs in water (including the cumulative distribution curves of particle size). Dissolution profile of CUR in (**C**) pH 1.2, (**D**) pH 6.8 buffer solutions each containing 0.2% Tween 80 at 37°C. ■, CUR, ●, CUR/Mog-V SDPs.

$$\delta_{obs}=\delta_{mic}-\left(\frac{CMC}{C}\right)\times(\delta_{mic}-\delta_{obs}) \quad (1)$$

Therefore, the fitting lines on both sides of the CMC can be obtained by plotting $\delta_{obs}$ against 1/C (Figure 4B). The value of CMC is corresponding to the intersection points. The CMC of Mog-V was calculated to be ~5.5 mg/mL.

The chemical shift changes were further used to find the aggregation number ($N_{agg}$) of Mog-V. If the molecules exist as monomers or aggregates (with given $N_{agg}$), the self-aggregation equilibrium model can be described as (Equation 2), where *K* represents the equilibrium constant, n represents the aggregation number, *M* and $M_n$ represent the monomer and micelle.

$$K = [M]^{(-n)}[M_n] \quad (2)$$

Equation (3) can be obtained by combining equations (1) and (2):

$$\log[C(\delta_{mon}-\delta_{obs})]= n\log[C(\delta_{obs}-\delta_{mic})]+\log(nK)+(1-n)\log(\delta_{mon}-\delta_{obs}) \quad (3)$$

According to (Equation 3), two fitting lines on both sides of the CMC can be obtained by plotting log $[C(\delta_{mon}- \delta_{obs})]$ against log $[C(\delta_{obs}- \delta_{mic})]$ (Figure 4C), and the slope of the fitting lines represented $N_{agg}$.[34] It was found that when the Mog-V concentration was below the CMC, the $N_{agg}$ was 2, implying dimer formation of Mog-V, while above the CMC, the $N_{agg}$ of Mog-V was 8.

To further investigate the aggregation behaviour of Mog-V in water, the structure of Mog-V molecules in non-aggregated and aggregated states was examined by using 2D $^1$H-$^1$H nuclear Overhauser Effect Spectroscopy (NOESY).[35] The nuclear Overhauser effect (NOE) is the transfer of nuclear spin polarisation from one population of spin-active nuclei to another. NOE is an important NMR parameter for conformational analysis, as the magnitude of the NOE is

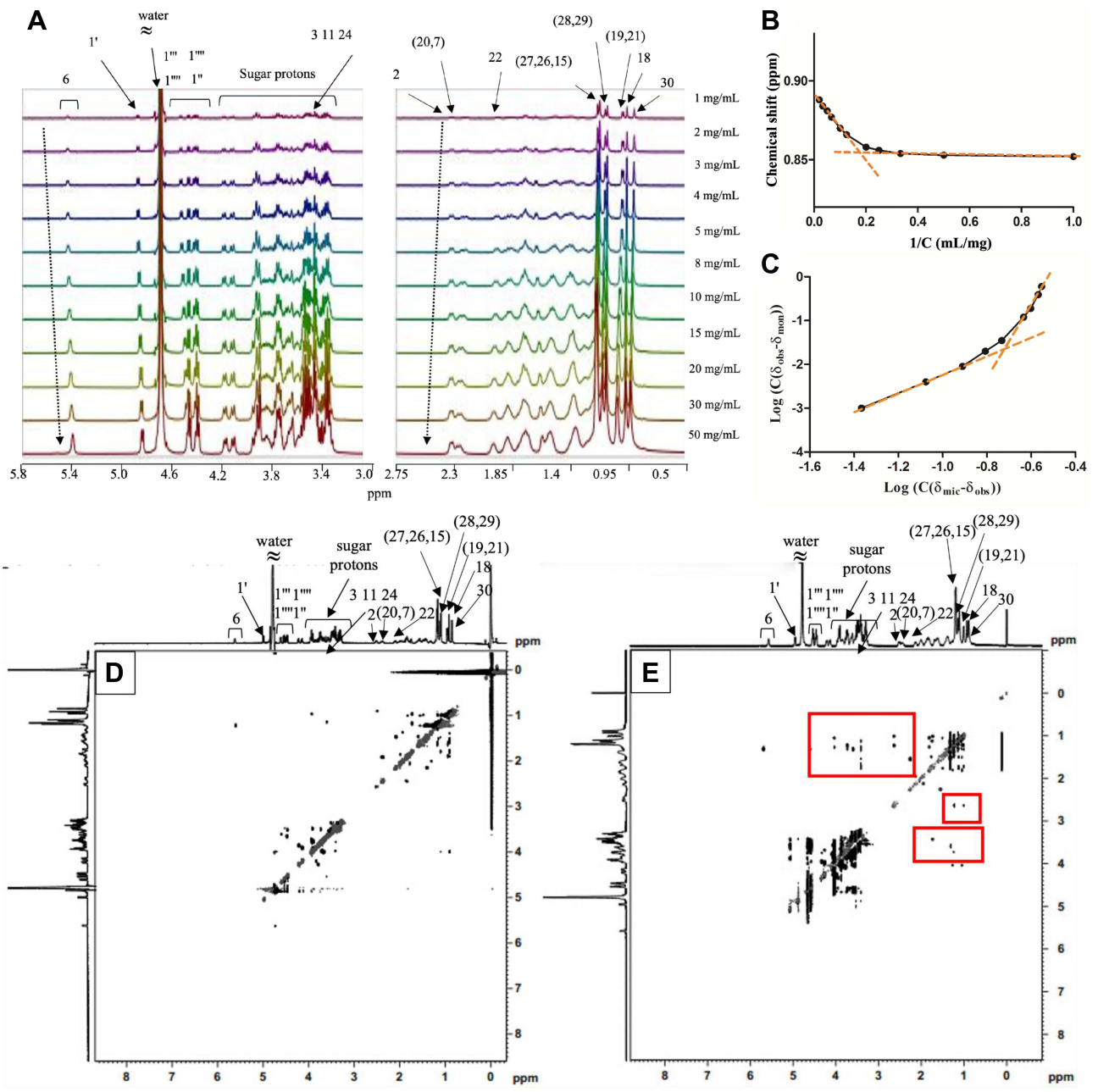


**Figure 4** $^1$H NMR spectra of Mog-V solution at concentrations of 1–50 mg/mL recorded in $D_2O$ (**A**). Plots of (**B**) $\delta_{obs}$ against 1/C and (**C**) log ($C(\delta_{obs}-\delta_{mon})$) against log ($C(\delta_{mic}-\delta_{obs})$) for the H-30 peak from the $^1$H NMR spectra. 2D $^1$H-$^1$H NOESY spectra of Mog-V at (**D**) 1 mg/mL (below CMC) and (**E**) 50 mg/mL (above CMC).

inversely proportional to the interproton distance. In NOESY, the NOE is manifested as a cross-peak between two resonances indicating that the two protons are near in space.

For the Mog-V solution of 1 mg/mL, its NOESY spectrum showed a few weak cross-peaks only among sugar proton pairs, which could be ascribed to intramolecular interaction (Figure 4D). However, we did not observe any NOE cross-peaks between the glucose group and the basic skeleton protons of Mog-V. The results showed that the Mog-V was likely in a non-aggregated state. The result is expected as the CMC of Mog-V was ~5.5 mg/mL. At such low concentration of 1 mg/mL, Mog-V molecules are in free form.

When the concentration of Mog-V increased to 50 mg/mL, additional correlation peaks were observed (Figure 4E), indicating dense packing of the molecules in the aggregates. Most of the new cross-peaks appeared in the hydrophobic

region, which can be ascribed to the hydrophobic core formation, implying the hydrophobic interaction of the tetracyclic triterpenoid skeleton of the Mog-V molecule. At the same time, the cross-peak intensity of sugar protons among hydrophilic portion was increased in comparison with that under the non-aggregated state. It is worth noting that there were no NOE interactions between tetracyclic triterpenoids skeleton and the hydrophilic portion of the Mog-V.

Collectively, these results showed that Mog-V molecules self-associated into micelles at higher concentrations, with the tetracyclic triterpenoids skeleton forming a hydrophobic core, and surrounding sugar groups forming the shell, as depicted in Figure 1C. The core-shell structure provided the mechanism of solubilising compounds with poor water solubility.

In our previous studies, it was shown that micelles of glucosides played an important role in the improvement of the apparent solubility of drugs.[16–18] Moreover, the nanostructure of micelles self-assembled by various glucosides displayed different properties. For example, the CMC of Rutin-G was 5 mg/mL, while that of Stevia-G was 12 mg/mL; the aggregation number of Rutin-G above the CMC was 4, while that of Stevia-G was 12. In the current study, the CMC of Mog-V was found to be 5.5 mg/L and the aggregation number was 8, when the concentraion is above CMC. Thus, it is necessary to study the properties of nanosized micelles and aggregation behaviour of glucosides during the formulation development process.

## Solubilisation Mechanism of CUR

To understand the interaction of Mog-V with CUR in water, the $^{1}$H NMR and 2D $^{1}$H-$^{1}$H NOESY NMR spectra of Mog-V and CUR/Mog-V SDPs were recorded (Figure 5). In $^{1}$H NMR spectra, the peaks of CUR from SDPs were clearly detected, indicating CUR was in molecular-dispersed state rather than crystal state. Furthermore, the proton peaks of the tetracyclic triterpenoid skeleton (H-3, 6, 11, 15, 19, 21, 24, 26, 27, 28, and 29) from SDPs exhibited upfield shifts compared with that of the untreated Mog-V, while the glucose protons showed no significant change.

This result revealed the interaction of the tetracyclic triterpenoid skeleton of Mog-V with CUR. In the 2D $^{1}$H-$^{1}$H NOESY NMR spectra, the key NOE cross peaks, used to infer the possible interaction sites between Mog-V

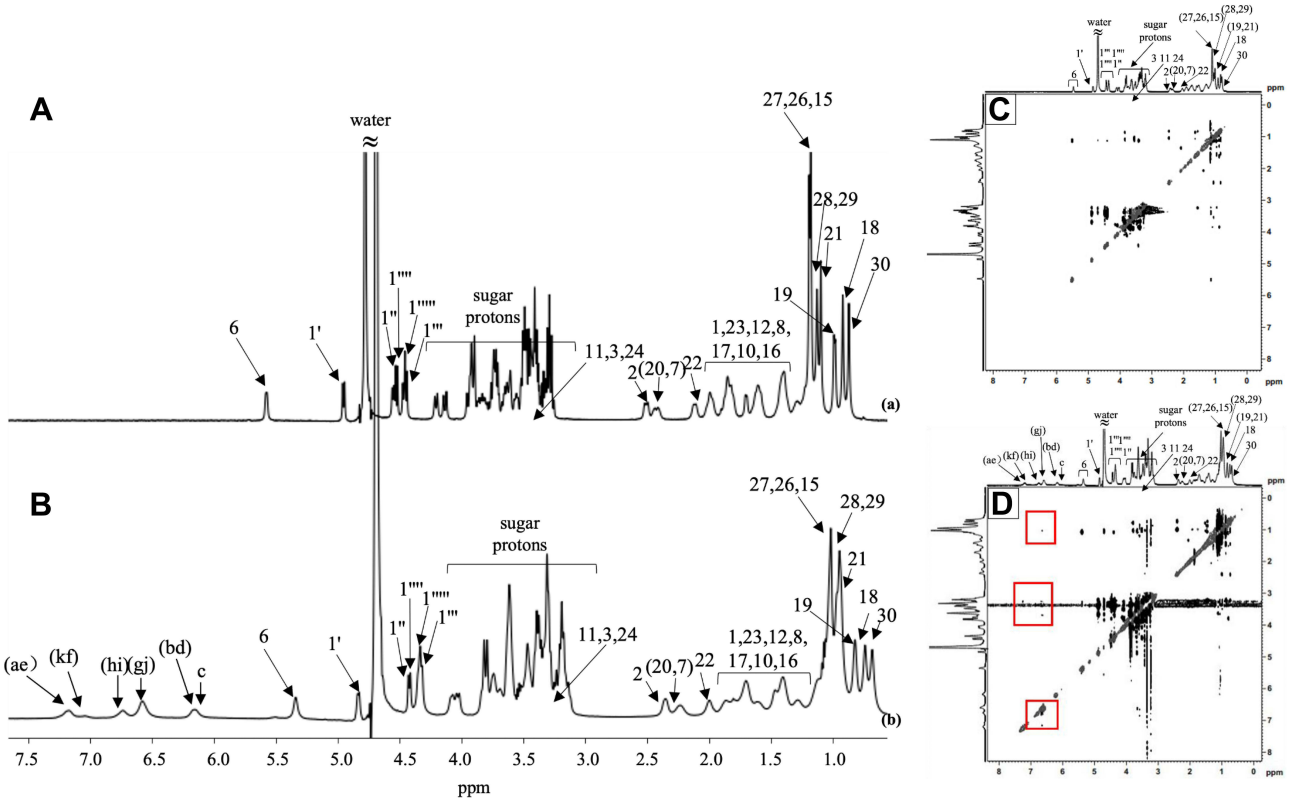


**Figure 5** $^{1}$H NMR spectra of (**A**) Mog-V, 50 mg/mL; (**B**) CUR/Mog-V SDPs, 55 mg/mL. 2D $^{1}$H-$^{1}$H NOESY spectra of (**C**) Mog-V and (**D**) CUR/Mog-V SDPs.

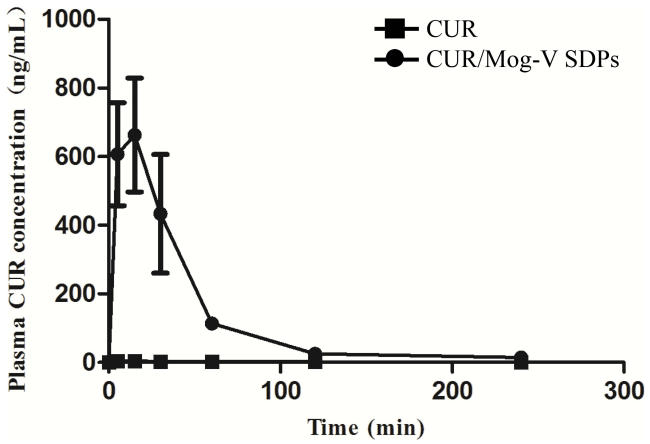


**Figure 6** Plasma concentration-time profiles in rats after oral administration of CUR crystal and CUR/Mog-V SDPs. ■, CUR; ●, CUR/Mog-V SDPs. N = 4.

and CUR, are marked. The aromatic protons and olefinic protons of the CUR (a, b, d, e, g, h, i and j) exhibited NOE correlations with those of the tetracyclic triterpenoid skeleton (H-3, 6, 11, 15, 19, 21, 24, 26, 27, 28, and 29) of Mog-V. In contrast, there were no NOE cross-peaks between the CUR protons and the glucose units of Mog-V. Taken together, the NOE interactions showed that CUR was solubilised due to the inclusion into the Mog-V hydrophobic core of Mog-V micelles.

## Oral Absorption of CUR Crystal and SDPs in Rats

To evaluate the oral absorption of CUR, the CUR powders and CUR/Mog-V SDPs were administered to rats, respectively, at the same dose of 100 mg CUR/kg. The plasma concentration–time profiles of CUR are shown in Figure 6 and Table 3. The plasma concentration of CUR/Mog-V SDP group rapidly reached a maximum of 663.1 ± 331 ng/mL at 15 min, which was 111-fold higher than that of CUR group. The area under the curve ($AUC_{0-t}$) obtained for CUR/Mog-V SDPs was 29-fold higher than that of CUR group.

The significant increase ($p < 0.05$) of both $C_{max}$ and $AUC_{(0-t)}$ clearly demonstrated the effectiveness of Mog-V for enhancing the oral absorption of CUR.

The oral absorption results are consistent with those obtained in the dissolution study, in which CUR dissolved much faster and achieved higher solubility in SDPs compared with CUR powders. With more solubilised CUR molecules in the Mog-V micelles, the CUR can be better absorbed into blood circulation, possible via passive diffusion mechanism. Additionally, the results also indicated that the SDPs are a useful formulation for oral delivery of CUR.

# Conclusion

It was shown that, CUR and Mog-V can form a solid dispersion at a ratio of 1:10. When dissolved in water, the solid dispersion self-assembled into Mog-V micelles to solubilise CUR by nearly 6000-fold. The CMC of Mog-V was found to be 5.5 mg/mL, and the aggregation number was 8 when the concentration was above CMC. With a diameter of ~160 nm, the Mog-V micelles exhibited a core-shell structure, in which the tetracyclic triterpenoid skeleton was segregated from

**Table 3** The Oral Absorption of CUR Crystal and CUR/Mog-V SDPs in Rats

| Group | $C_{max}$ (ng/mL) | $T_{max}$ (min) | $AUC_{0-t}$ (μg min/L) |
|---|---|---|---|
| CUR/Mog-V SDPs | 663.1±331 | 15±0 | 45,665±14,926 |
| CUR crystal | 5.992±3.6 | 10±5.8 | 1577±491 |

**Note**: Data represent the rean ± SD of 4 rats.
**Abbreviations**: $C_{max}$, Maximum CUR concentration in plasma; $T_{max}$, Time to maximum concentration; $AUC_{0-T}$, Area under the curve.

the aqueous exterior to form a core to encapsulate CUR. In rats, the solid dispersion increased the oral absorption of CUR by 29-fold compared with CUR crystals. Mog-V can be a useful carrier to increase the solubility of hydrophobic molecules, such as CUR.

## Acknowledgment

This work was supported by the National Natural Science Foundation of China (81473357 and 82074128), the Open Project Program of NMPA Key Laboratory for Impurity Profile of Chemical Drugs (NMPA-KLIPCD-2020-01), the Project of Jiangsu Administration for Market Regulation (KJ207558), Yunnan Wu Chunyong Expert Workstation Project, and the China Pharmaceutical University Double First-Class Initiative (CPU2022QZ16).

## Disclosure

The authors report no conflicts of interest in this work.

## References

1. Degot P, Huber V, Hofmann E, Hahn M, Touraud D, Kunz W. Solubilization and extraction of curcumin from Curcuma Longa using green, sustainable, and food-approved surfactant-free microemulsions. *Food Chem*. 2021;336:127660. doi:10.1016/j.foodchem.2020.127660
2. Fu DW, Fu JJ, Li JJ, et al. Efficient encapsulation of curcumin into spent brewer's yeast using a pH-driven method. *Food Chem*. 2022;394:133537. doi:10.1016/j.foodchem.2022.133537
3. Chin KY. The spice for joint inflammation: anti-inflammatory role of curcumin in treating osteoarthritis. *Drug Des Devel Ther*. 2016;10:3029–3042. doi:10.2147/DDDT.S117432
4. Abrahams S, Haylett WL, Johnson G, Carr JA, Bardien S. Antioxidant effects of curcumin in models of neurodegeneration, aging, oxidative and nitrosative stress: a review. *Neuroscience*. 2019;406:1–21. doi:10.1016/j.neuroscience.2019.02.020
5. Walker BC, Mittal S. Antitumor Activity of Curcumin in Glioblastoma. *Int J Mol Sci*. 2020;21(24). doi:10.3390/ijms21249435
6. Reyhaneh M-M, Hassanian SM, Rahmani F, et al. Phytosomal curcumin elicits anti-tumor properties through suppression of angiogenesis, cell proliferation and induction of oxidative stress in colorectal cancer. *Curr Pharm Des*. 2018;24:4626.
7. Yu H, Huang Q. Investigation of the absorption mechanism of solubilized curcumin using Caco-2 cell monolayers. *J Agric Food Chem*. 2011;59 (17):9120–9126. doi:10.1021/jf201451m
8. Shin MS, Yu JS, Lee J, et al. A hydroxypropyl methylcellulose-based solid dispersion of curcumin with enhanced bioavailability and its hepatoprotective activity. *Biomolecules*. 2019;9(7). doi:10.3390/biom9070281
9. Mashaqbeh H, Obaidat R, Al-Shar'i N. Evaluation and characterization of curcumin-beta-cyclodextrin and cyclodextrin-based nanosponge inclusion complexation. *Polymers*. 2021;13(23). doi:10.3390/polym13234073
10. Cui J, Zhou J, Huang L, Jing J, Wang N, Wang L. Curcumin encapsulation and protection based on lysozyme nanoparticles. *Food Sci Nutr*. 2019;7 (8):2702–2707. doi:10.1002/fsn3.1129
11. Feng T, Wei Y, Lee RJ, Zhao L. Liposomal curcumin and its application in cancer. *Int J Nanomedicine*. 2017;12:6027–6044. doi:10.2147/IJN.S132434
12. Ganguly R, Kunwar A, Dutta B, et al. Heat-induced solubilization of curcumin in kinetically stable pluronic P123 micelles and vesicles: an exploit of slow dynamics of the micellar restructuring processes in the aqueous pluronic system. *Colloids Surf B Biointerfaces*. 2017;152:176–182. doi:10.1016/j.colsurfb.2017.01.023
13. Butnariu M, Quispe C, Koirala N, et al. Bioactive effects of curcumin in human immunodeficiency virus infection along with the most effective isolation techniques and type of nanoformulations. *Int J Nanomedicine*. 2022;17:3619–3632. doi:10.2147/IJN.S364501
14. Ghezzi M, Pescina S, Padula C, et al. Polymeric micelles in drug delivery: an insight of the techniques for their characterization and assessment in biorelevant conditions. *J Control Release*. 2021;332:312–336. doi:10.1016/j.jconrel.2021.02.031
15. Zhang Q, Polyakov NE, Chistyachenko YS, et al. Preparation of curcumin self-micelle solid dispersion with enhanced bioavailability and cytotoxic activity by mechanochemistry. *Drug Deliv*. 2018;25(1):198–209. doi:10.1080/10717544.2017.1422298
16. Zhang J, Tozuka Y, Uchiyama H, et al. NMR investigation of a novel excipient, alpha-glucosylhesperidin, as a suitable solubilizing agent for poorly water-soluble drugs. *J Pharm Sci*. 2011;100(10):4421–4431. doi:10.1002/jps.22606
17. Tozuka Y, Higashi K, Morita T, et al. Transglycosylated rutin-specific non-surface-active nanostructure affects absorption enhancement of flurbiprofen. *Eur J Pharm Biopharm*. 2012;82(1):120–126. doi:10.1016/j.ejpb.2012.05.005
18. Zhang J, Higashi K, Ueda K, et al. Drug solubilization mechanism of alpha-glucosyl stevia by NMR spectroscopy. *Int J Pharm*. 2014;465(1–2):255–261. doi:10.1016/j.ijpharm.2014.01.035
19. Luo Y, Gong C, Wei M, et al. Evaluation of mogroside V as a promising carrier in drug delivery: improving the bioavailability and liver distribution of silybin. *AAPS Pharm Sci Tech*. 2020;21(4):123. doi:10.1208/s12249-020-01645-9
20. Zhang F, Koh GY, Jeansonne DP, et al. A novel solubility-enhanced curcumin formulation showing stability and maintenance of anticancer activity. *J Pharm Sci*. 2011;100(7):2778–2789. doi:10.1002/jps.22512
21. Pawar RS, Krynitsky AJ, Rader JI. Sweeteners from plants—with emphasis on Stevia rebaudiana (Bertoni) and Siraitia grosvenorii (Swingle). *Anal Bioanal Chem*. 2013;405(13):4397–4407.
22. Suez J, Korem T, Zeevi D, et al. Artificial sweeteners induce glucose intolerance by altering the gut microbiota. *Nature*. 2014;514(7521):181–186. doi:10.1038/nature13793
23. Suez J, Cohen Y, Valdes-Mas R, et al. Personalized microbiome-driven effects of non-nutritive sweeteners on human glucose tolerance. *Cell*. 2022. doi:10.1016/j.cell.2022.07.016

24. Jia Z, Yang X. A minor, sweet cucurbitane glycoside from Siraitia grosvenorii. *Nat Prod Commun*. 2009;4(6):769–772.
25. Poppler AC, Lubtow MM, Schlauersbach J, Wiest J, Meinel L, Luxenhofer R. Loading-dependent structural model of polymeric micelles encapsulating curcumin by solid-state NMR spectroscopy. *Angew Chem Int Ed Engl*. 2019;58(51):18540–18546. doi:10.1002/anie.201908914
26. Bhujbal SV, Mitra B, Jain U, et al. Pharmaceutical amorphous solid dispersion: a review of manufacturing strategies. *Acta Pharm Sin B*. 2021;11(8):2505–2536. doi:10.1016/j.apsb.2021.05.014
27. Hancock BC, Zografi G. Characteristics and significance of the amorphous state in pharmaceutical systems. *J Pharm Sci*. 1997;86:1.
28. Metre S, Mukesh S, Samal SK, Chand M, Sangamwar AT. Enhanced biopharmaceutical performance of rivaroxaban through polymeric amorphous solid dispersion. *Mol Pharm*. 2018;15(2):652–668. doi:10.1021/acs.molpharmaceut.7b01027
29. Kadota K, Okamoto D, Sato H, Onoue S, Otsu S, Tozuka Y. Hybridization of polyvinylpyrrolidone to a binary composite of curcumin/alpha-glucosyl stevia improves both oral absorption and photochemical stability of curcumin. *Food Chem*. 2016;213:668–674. doi:10.1016/j.foodchem.2016.07.025
30. Dedroog S, Pas T, Vergauwen B, Huygens C, Van den Mooter G. Solid-state analysis of amorphous solid dispersions: why DSC and XRPD may not be regarded as stand-alone techniques. *J Pharm Biomed Anal*. 2020;178:112937. doi:10.1016/j.jpba.2019.112937
31. Aditya NP, Hamilton IE, Norton IT. Amorphous nano-curcumin stabilized oil in water emulsion: physico chemical characterization. *Food Chem*. 2017;224:191–200. doi:10.1016/j.foodchem.2016.12.082
32. Shimizu S, Pires PAR, Fish H, Halstead TK, El Seoud OA. Proton and carbon-13 NMR study of the aggregation of benzyl(2-acylaminoethyl) dimethylammonium chloride surfactants in D2O. *Phys Chem Chem Phys*. 2003;5(16). doi:10.1039/b303622g
33. Andrade-Dias C, Lima S, Teixeira-Dias JJ. From simple amphiphilic to surfactant behavior: analysis of (1)H NMR chemical shift variations. *J Colloid Interface Sci*. 2007;316(1):31–36. doi:10.1016/j.jcis.2007.07.049
34. Luchetti L, Mancini G. NMR investigation on the various aggregates formed by a gemini chiral surfactant. *Langmuir*. 2000;16(1):161–165. doi:10.1021/la990713z
35. Makriyannis A, Pavlopoulos S. Structural chemistry using NMR spectroscopy, pharmaceuticals. *Encyclopedia Spectroscopy Spectrometry*. 1999;8:2261–2271.
36. Song IS, Cha JS, Choi MK. Characterization, in vivo and in vitro evaluation of solid dispersion of curcumin containing d-alpha-tocopheryl polyethylene glycol 1000 succinate and mannitol. *Molecules*. 2016;21(10). doi:10.3390/molecules21101386
37. More SK, Pawar AP. Preparation, optimization and preliminary pharmacokinetic study of curcumin encapsulated turmeric oil microemulsion in zebra fish. *Eur J Pharm Sci*. 2020;155:105539. doi:10.1016/j.ejps.2020.105539
38. Ji H, Tang J, Li M, Ren J, Zheng N, Wu L. Curcumin-loaded solid lipid nanoparticles with Brij78 and TPGS improved in vivo oral bioavailability and in situ intestinal absorption of curcumin. *Drug Deliv*. 2016;23(2):459–470. doi:10.3109/10717544.2014.918677
39. Chen H, Wu J, Sun M, et al. N-trimethyl chitosan chloride-coated liposomes for the oral delivery of curcumin. *J Liposome Res*. 2012;22(2):100–109. doi:10.3109/08982104.2011.621127
40. Ji-Jin GU, Deng YJ. Preparation of curcumin liposomes and its oral pharmacokinetics in rats. *J Chengdu Med Colle*. 2010;5:97–100.
41. Tozuka Y, Kishi J, Takeuchi H. Anomalous dissolution property enhancement of naringenin from spray-dried particles with α-glucosylhesperidin. *Adv Powder Tech*. 2010;21(3):305–309. doi:10.1016/j.apt.2009.12.013
42. Uchiyama H, Tozuka Y, Imono M, Takeuchi H. Improvement of dissolution and absorption properties of poorly water-soluble drug by preparing spray-dried powders with alpha-glucosyl hesperidin. *Int J Pharm*. 2010;392(1–2):101–106. doi:10.1016/j.ijpharm.2010.03.037
43. Uchiyama H, Tozuka Y, Imono M, Takeuchi H. Transglycosylated stevia and hesperidin as pharmaceutical excipients: dramatic improvement in drug dissolution and bioavailability. *Eur J Pharm Biopharm*. 2010;76(2):238–244. doi:10.1016/j.ejpb.2010.07.006
44. Tozuka Y, Imono M, Uchiyama H, Takeuchi H. A novel application of alpha-glucosyl hesperidin for nanoparticle formation of active pharmaceutical ingredients by dry grinding. *Eur J Pharm Biopharm*. 2011;79(3):559–565. doi:10.1016/j.ejpb.2011.07.006
45. Sato H, Fujimori M, Suzuki H, et al. Absorption improvement of tranilast by forming highly soluble nano-size composite structures associated with alpha-glucosyl rutin via spray drying. *Eur J Pharm Biopharm*. 2015;92:49–55. doi:10.1016/j.ejpb.2015.02.021
46. Fujimori M, Kadota K, Kato K, et al. Low hygroscopic spray-dried powders with trans-glycosylated food additives enhance the solubility and oral bioavailability of ipriflavone. *Food Chem*. 2016;190:1050–1055. doi:10.1016/j.foodchem.2015.06.081
47. Kadota K, Semba K, Shakudo R, et al. Inhibition of photodegradation of highly dispersed folic acid nanoparticles by the antioxidant effect of transglycosylated rutin. *J Agric Food Chem*. 2016;64(15):3062–3069. doi:10.1021/acs.jafc.6b00334
48. Tozuka Y, Imono M, Uchiyama H, et al. Dry powder formulation with α-glycosyltransferase-treated stevia for the effective absorption of hydrophobic bioactive compounds in crude drugs. *Powder Tech*. 2013;240:2–6. doi:10.1016/j.powtec.2012.07.014
49. Uchiyama H, Tozuka Y, Asamoto F, Takeuchi H. Fluorescence investigation of a specific structure formed by aggregation of transglycosylated stevias: solubilizing effect of poorly water-soluble drugs. *Eur J Pharm Sci*. 2011;43(1–2):71–77. doi:10.1016/j.ejps.2011.03.014
50. Fujimori M, Kadota K, Tozuka Y. Mixed micelle system produced by interaction between transglycosylated stevia and an ionic surfactant improves dissolution profile of mefenamic acid. *J Pharm Sci*. 2017;106(4):1117–1123. doi:10.1016/j.xphs.2016.12.024
51. Uchiyama H, Wada Y, Hatanaka Y, et al. Solubility and permeability improvement of quercetin by an interaction between alpha-glucosyl stevia nanoaggregates and hydrophilic polymer. *J Pharm Sci*. 2019;108(6):2033–2040. doi:10.1016/j.xphs.2019.01.007
52. Wan ZL, Wang JM, Wang LY, Yang XQ, Yuan Y. Enhanced physical and oxidative stabilities of soy protein-based emulsions by incorporation of a water-soluble stevioside-resveratrol complex. *J Agric Food Chem*. 2013;61(18):4433–4440. doi:10.1021/jf4003945
53. Wang H, He Y, Hou Y, Geng Y, Wu X. Novel self-nanomicellizing formulation based on Rebaudioside A: a potential nanoplatform for oral delivery of naringenin. *Mater Sci Eng C Mater Biol Appl*. 2020;112:110926. doi:10.1016/j.msec.2020.110926
54. Uchiyama H, Dowaki M, Kadota K, Arima H, Sugiyama K, Tozuka Y. Single-stranded beta-1,3-1,6-glucan as a carrier for improved dissolution and membrane permeation of poorly water-soluble compounds. *Carbohydr Polym*. 2020;247:116698. doi:10.1016/j.carbpol.2020.116698
55. Uchiyama H, Kadota K, Nakanishi A, Tandia M, Tozuka Y. A simple blending with alpha-glycosylated naringin produces enhanced solubility and absorption of pranlukast hemihydrate. *Int J Pharm*. 2019;567:118490. doi:10.1016/j.ijpharm.2019.118490